

Aberystwyth University

Correlating weathered, microphenocryst-rich, intermediate tephra

Pearce, Nick; Alloway, Brent V.; Wickham, Craig

Published in:

Quaternary International

DOI:

[10.1016/j.quaint.2019.01.017](https://doi.org/10.1016/j.quaint.2019.01.017)

Publication date:

2019

Citation for published version (APA):

Pearce, N., Alloway, B. V., & Wickham, C. (2019). Correlating weathered, microphenocryst-rich, intermediate tephra: An approach combining bulk and single shard analyses from the Lepu  Tephra, Chile and Argentina. *Quaternary International*, 500, 71-82. <https://doi.org/10.1016/j.quaint.2019.01.017>

General rights

Copyright and moral rights for the publications made accessible in the Aberystwyth Research Portal (the Institutional Repository) are retained by the authors and/or other copyright owners and it is a condition of accessing publications that users recognise and abide by the legal requirements associated with these rights.

- Users may download and print one copy of any publication from the Aberystwyth Research Portal for the purpose of private study or research.
- You may not further distribute the material or use it for any profit-making activity or commercial gain
- You may freely distribute the URL identifying the publication in the Aberystwyth Research Portal

Take down policy

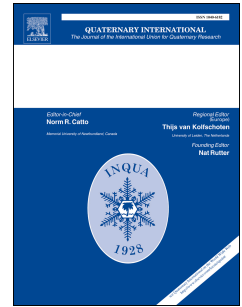
If you believe that this document breaches copyright please contact us providing details, and we will remove access to the work immediately and investigate your claim.

tel: +44 1970 62 2400
email: is@aber.ac.uk

Accepted Manuscript

Correlating weathered, microphenocryst-rich, intermediate tephra: An approach combining bulk and single shard analyses from the Lepué Tephra, Chile and Argentina

Nicholas J.G. Pearce, Brent V. Alloway, Craig Wickham



PII: S1040-6182(18)31087-5

DOI: <https://doi.org/10.1016/j.quaint.2019.01.017>

Reference: JQI 7714

To appear in: *Quaternary International*

Received Date: 26 September 2018

Revised Date: 12 January 2019

Accepted Date: 13 January 2019

Please cite this article as: Pearce, N.J.G., Alloway, B.V., Wickham, C., Correlating weathered, microphenocryst-rich, intermediate tephra: An approach combining bulk and single shard analyses from the Lepué Tephra, Chile and Argentina, *Quaternary International* (2019), doi: <https://doi.org/10.1016/j.quaint.2019.01.017>.

This is a PDF file of an unedited manuscript that has been accepted for publication. As a service to our customers we are providing this early version of the manuscript. The manuscript will undergo copyediting, typesetting, and review of the resulting proof before it is published in its final form. Please note that during the production process errors may be discovered which could affect the content, and all legal disclaimers that apply to the journal pertain.

1 **Correlating weathered, microphenocryst-rich, intermediate tephra: an approach combining bulk**
2 **and single shard analyses from the Lepu  Tephra, Chile and Argentina.**

3 Nicholas J.G. Pearce^{1,*}, Brent V. Alloway^{2,3}, Craig Wickham^{1,4}

4 1. Department of Geography & Earth Sciences, Aberystwyth University, SY23 3DB, Wales, UK

5 2. School of Environment, University of Auckland, Private Bag 92019, Auckland, New Zealand

6 3. Centre for Archaeological Science (CAS), School of Earth and Environmental Sciences, University of
7 Wollongong, NSW 2522, Australia

8 4. Present address: SRK Consulting, Churchill Way, Cardiff, CF10 2HH, Wales, UK

9 *Corresponding author: Nick.Pearce@aber.ac.uk

10 ***Submission for the Quaternary International "500" volume***

11 **Abstract.**

12 Chemical correlation of intermediate tephra deposits using microanalytical data is problematic
13 because (i) the phenocryst content of their component glass shards affects major and trace element
14 analyses (ii) bulk chemistry can be affected by variations in mineral/lithic components across the fall-
15 out, and (iii) weathering readily alters their composition. All of these problems affect the Lepu 
16 Tephra, a prominent marker horizon extensively distributed across the Los Lagos Region of Chile and
17 the Chile-Argentina frontier in north-western Patagonia, which was erupted from Volc n
18 Michinmahuida at c. 11000 cal a BP. Weathering of terrestrial cover-bed deposits in this hyper-
19 humid depositional environment leaves only a few occurrences of the tephra which contain fresh
20 glass shards for microbeam analysis, but their highly phenocrystic nature makes data interpretation
21 difficult. Equally, leaching of mobile elements during weathering causes considerable compositional
22 changes across the fall-out region and is evident in bulk sample analyses. Elements such as the REE
23 and Y, generally regarded as immobile, show marked mobility. Within the REE, the development of
24 "M-type" tetrad effects and positive Ce-anomalies result from a combination of dissolution/leaching
25 of the REE from the bulk sample and retention by co-precipitation of Ce⁴⁺ on Fe-oxyhydroxides in
26 this high-rainfall, hyper-humid, oxic environment. Chemical correlation of the Lepu  Tephra is thus
27 not straightforward. However, by careful consideration of the data for a limited range of elements,
28 chemical correlation can be achieved using elements which (i) are incompatible in magmatic systems
29 (and thus their ratios are unaffected by the presence of phenocrysts in single glass shard microbeam
30 analysis) and (ii) are not mobilised in these weathering conditions. These elements are Zr, Hf, Nb, Ta
31 and Th. Their ratios (i) allow for the comparison of single grain and bulk sample analyses, extending
32 the geographic range over which data can be compared for the Lepu  Tephra, (ii) provide a robust

33 chemical correlation of this weathered, intermediate tephra deposit, enabling correlation even
34 where elements traditionally considered immobile (REE, Y, and U) have been significantly mobilised,
35 and (iii) allow the Lepué Tephra to be distinguished from other local tephra deposits. This combined
36 analytical approach enables tephtras that have been variably weathered to become useful marker
37 beds over much wider geographical areas than previously feasible, thereby enhancing their
38 tephrochronological application in Quaternary research.

39 **Keywords.**

40 Lepué Tephra; tephrochronology; tephra correlation; REE geochemistry; REE tetrad effect; immobile
41 elements; incompatible elements

42
43 **1. Introduction**

44 Correlation of intermediate tephra deposits using compositional data can be highly problematic
45 because of the phenocrystic nature of the magma, compositional variation in the magma erupted
46 from zoned magma chambers, and because these intermediate bulk compositions can alter rapidly,
47 whereby the glass phase analyses can be compromised (Alloway et al., 1995; Riehle et al., 1999;
48 Shane, 2005; Donoghue et al., 2007; Lowe et al., 2008). In part for these reasons andesitic tephra
49 have often been overlooked in favour of compositional correlation studies which suffer less from
50 these issues, e.g. using rhyolitic tephra which are often more widespread, or basaltic tephra, often
51 less widespread but erupted frequently in areas such as the North Atlantic from Iceland (Abbott et
52 al., 2013). Specifically, single glass shard analyses by micro-beam methods for major and trace
53 elements of intermediate tephra (i.e. basaltic-andesite and andesite) are often hampered by the
54 presence of abundant phenocrysts which can contribute to the analysis of a “glass” shard (Platz et
55 al., 2007; Lowe, 2011). This phenocryst effect is especially problematic in laser ablation (LA) ICP-MS
56 analysis, where the analysed volume is much greater than in electron probe microanalysis (EPMA).
57 Any analysed material from phenocrystic shards with a “bulk” intermediate composition is highly
58 likely to include phenocrysts, notably plagioclase, which adds Ca and Sr to the analysed material and
59 dilutes the concentration of incompatible elements from the glass phase, which may be dacitic or
60 rhyolitic in composition. These incompatible elements are often very useful in tephra correlation
61 (Pearce et al., 2002; Pearce et al., 2004; Pearce et al., 2007; Pearce et al., 2011; Pearce, 2014; Pearce
62 et al., 2014). Bulk analyses of intermediate tephra, however, can be useful in that they overcome the
63 problem of analysis of variable quantities of phenocrysts with grain-specific methods, but bulk
64 analyses can incorporate xenolithic/xenocrystic material from the eruption, or enclosing sediment
65 intermixed during deposition, and thus require careful sampling. To further complicate their

66 correlation, bulk tephra composition may change with distance from the vent because of
67 sedimentary fractionation of the erupted material (Sarna-Wojcicki et al., 1981; Juvigné and Porter,
68 1985). Additionally, intermediate (andesitic) tephra weathers comparatively rapidly (Kirkman and
69 McHardy, 1980; Parfitt et al., 1983; Alloway et al., 1995; Churchman and Lowe, 2012) and
70 consequently analysis and correlation may be further hindered by processes occurring in the soil-
71 forming environment (Cronin et al., 1996; McHenry et al., 2008; Lowe, 2011; Lowe et al., 2017).
72 These factors make the direct comparison of bulk and single grain analyses difficult because of the
73 effect mixing variable proportions of glass with phenocrysts during microbeam analysis can have on
74 single grain data, as well as other compositional effects from lithics or contaminant phases.
75 However, when chosen with care, the use of appropriate element ratios can overcome some of
76 these issues (Pearce et al., 2002; Pearce et al., 2004; Lowe et al., 2017; Martin-Jones et al., 2017b).
77 Here, data from the Lepué Tephra, deposited from a large, early Holocene eruption of Volcán
78 Michinmahuida in the Andean Southern Volcanic Zone of Chile, is used to illustrate several of these
79 problems, and to show how, despite significant challenges related to the physical properties of this
80 deposit, chemical correlation can be achieved in the most unfavourable (analytical and geochemical)
81 conditions. This approach may offer a method for correlation of proximal to distal deposits where
82 preservation varies, and where alteration has affected the concentrations of elements which are
83 generally considered to be immobile (e.g. the rare earth elements, REE). These findings therefore
84 provide a new way of making use of some tephra deposits which were previously considered to have
85 limited value as chronostratigraphic units, making them valuable marker beds over much wider
86 geographical areas, thereby enhancing their potential application to linking and dating deposits and
87 landscapes (i.e. tephrochronologically) in a range of associated Quaternary studies.

88

89 **2. Lepué Tephra: an introduction**

90 The Lepué Tephra, a prominent marker horizon described in detail by Alloway et al. (2017a), is
91 extensively distributed across the Los Lagos Region of Chile, and straddles the Chile-Argentina
92 frontier in northwest Patagonia (Figure 1). The Lepué Tephra can be correlated to an equivalent-
93 aged >40 m thick pyroclastic flow deposit (Amarillo Ignimbrite) which is well exposed on the south-
94 eastern flanks of Michinmahuida. The source vent or vents of these co-eruptive units (Amarillo
95 Ignimbrite and Lepué Tephra) is/are currently obscured by an extensive ice field which mantles the
96 Michinmahuida volcanic massif, an ice sheet which will have been considerably larger at the time of
97 this eruption.

98 **Figure 1 about here**

99 The Lepu  Tephra is well constrained at c. 11000 cal a BP from ¹⁴C dates from lake and soil cover-bed
100 sequences in the area (Alloway et al., 2017a), where it occurs as a deposit ranging from less than a
101 centimetre in thickness to the north of Lago Llanquihue, a few centimetres to a decimetre thick on
102 Isla Grande de Chilo  or in the vicinity of Puerto Montt, and up to (and more than) ~ 2 m in thickness
103 near the town of Chait n to the immediate WSW of Volc n Michinmahuida. Lake cores from across
104 the region record between 2 cm to 28 cm of Lepu  Tephra, and ODP core 1233D (Leg 202)
105 (Tiedemann et al., 2007) contains 12 cm of the tephra, ~260 km NW of Volc n Michinmahuida. The
106 Lepu  Tephra is almost invariably the lowest tephra observed stratigraphically in the post-glacial
107 cover-bed sequence in this area, closely overlying either glacial till/diamicton deposits from the Last
108 Glacial Maximum or local bedrock. Figure 2 illustrates the range of field occurrences from proximal
109 to distal of the Lepu  Tephra throughout northwest Patagonia. Lepu  Tephra underlies the Chana
110 Tephra (previously referred to as Cha-1, Naranjo and Stern, 2004), the ~9.7 ka eruption of Volc n
111 Chait n (see Figure 2F), although several intensely weathered scoriaceous lapilli tephra deposits
112 from other local volcanoes (presumably Volc nes Corcovado, Yate or Calbuco, see Figure 2C) may
113 intervene but these are as yet uncharacterised (Alloway et al., 2017b).

114 **Figure 2 about here**

115 The Lepu  Tephra has many characteristics typical of a phreatomagmatic eruptive from a
116 compositionally zoned magma body, and produces a complex and variable tephra deposit (Figure
117 2A). In sections close to Volc n Michinmahuida, proximal Lepu  Tephra is typically a compact, dark
118 grey to brownish-grey, poorly sorted, massive to weakly stratified, scoriaceous lapilli to lapilli-tuff
119 (i.e. a consolidated lapilli tuff) of basaltic–andesitic bulk composition which often contains
120 accretionary lapilli up to ~3 cm in diameter (Figure 2B). This sometimes overlies a prominent
121 decimetre-thick red-brown medium-coarse (lapilli-size) scoriaceous fall unit from a magmatic phase
122 of the same eruption (Figure 2A). The combination of these textural features and variable sorting of
123 the deposit suggested to Alloway et al. (2017a) that variable interaction with significant quantities of
124 water during the eruption (Zimanowski, 2001) resulted in a complex intermixing of magmatic and
125 phreatomagmatic eruptive components (Cas and Wright, 1987), with the water here largely derived
126 from melting of the overlying ice cap. In places close to the source, the typical, massive accretionary
127 lapilli-tuff overlies a basal rhyolitic ash and a surge unit containing moderately sorted, inclined planar
128 to low-angle cross-bedded, scoriaceous ash and lapilli beds (not illustrated here, but see Alloway et
129 al., 2017a). At intermediate distances (between ~30 km to 60 km from Volc n Michinmahuida), the
130 Lepu  Tephra is between ~30 cm to 100 cm in thickness and typically is characterized by a
131 decimetre-thick weakly stratified, brownish grey, very poorly sorted cemented ash with indistinct
132 centimetre-sized accretionary lapilli and scoriaceous lapilli-rich ashy intra-beds (Figures 2B and 2C).

133 Distally, >~60 km to 100 km from the source, the Lepu  Tephra is deposited across much of Isla
134 Grande de Chilo  and its adjacent islands and the area around Puerto Montt (Figures 2D, 2E, 2F). In
135 Chilo  the Lepu  Tephra is the only macroscopic tephra that can be observed within the late last
136 glacial/post-glacial andic soil cover-beds, where it occurs as laterally discontinuous cemented
137 aggregates of olive-brown to reddish-brown fine to medium ash, and it typically closely overlies late
138 last glacial to Last Glacial Maximum (LGM)-aged colluvium, fluvio-glacial gravels and sands, and
139 glacial diamicts (till) (Figure 2E). Across this distal fallout region, the Lepu  Tephra can be hard to
140 observe within the andic (allophane- and ferrihydrite-rich) soil cover-beds as it forms highly
141 irregular, discontinuous pods of crudely bedded, cemented fine- to medium-ash enveloped by
142 similarly reddish-brown andic soil material (Figures 2E, 2F). This similarity with its enclosing
143 sediments allowed its distal extent to remain unrecognised in previous studies in the area (Naranjo
144 and Stern, 2004; Watt et al., 2011). Further details of the stratigraphic context and variations within
145 the Lepu  Tephra, along with details of all localities sampled for analysis in this study are given by
146 Alloway et al. (2017a), which should be consulted for details of the eruption and deposition history,
147 and major element chemical variation of the deposit, which are not reiterated here.

148

149 **3. Sampling and analytical data.**

150 The Lepu  Tephra was sampled extensively for chemical and mineralogical analysis of both bulk
151 material and single glass shards, across its visible fallout range and also from lake and ODP core
152 samples (see Figure 1). Proximal samples were relatively easy to sample with bulk samples of the
153 tephra being taken from the thick exposures. In addition, where present, accretionary lapilli were
154 sampled from these thicker proximal to medial deposits in the hope that they had accreted a near-
155 representative samples of the finer grained component of the bulk ash cloud material (Moore and
156 Peck, 1962; Gilbert and Lane, 1994). For distal deposits, the often rather hard, cemented nature of
157 the tephra made it possible to isolate small pods or biscuits of tephra (up to around 1-2 cm thick)
158 which were shaved of any obvious adhering soil material with a knife to leave "clean" centimetre-
159 sized pieces for analysis (see Figures 2E, 2F).

160 **Figure 3 about here**

161 Glass shards of the Lepu  Tephra were separated from three cover-bed sequences, four lake cores
162 and from ODP core 1233D, and prepared for analysis. Major elements were determined by EPMA at
163 the Victoria University of Wellington, New Zealand, with 15 kV accelerating voltage, 8 nA beam
164 current, and an electron beam defocused to between 20 to 10 μm . The same samples were
165 subsequently analysed by laser ablation LA-ICP-MS at Aberystwyth University, Wales using a 20 μm

166 diameter crater from a 193 nm Excimer laser operating at 10 J cm^{-2} and 5 Hz, and calibrated using
167 ^{29}Si as the internal standard against NIST SRM 612 and corrected for fractionation effects at the
168 laser-sample interface (Pearce et al., 1997; Pearce et al., 2011; Pearce, 2014). Figure 3 illustrates the
169 range of phenocryst content and vesicularity within the glass shards from the Lepu  Tephra,
170 dominated by plagioclase, with clinopyroxene and titanomagnetite. For many individual shards it is
171 difficult to impossible to place a 10-20 μm diameter analysis (either by EPMA or LA-ICP-MS) on pure
172 glass without encountering a phenocryst which will inevitably be included in the analysis. For both
173 major and trace element analyses, the MPI-DING reference material ATHO-G (Jochum et al., 2006)
174 was analysed as an unknown and gave both accurate and precise results ($\pm 5\text{-}10\%$ for trace elements;
175 between $\pm 1\text{-}10\%$ for major elements with the poorest analytical precision from the analyses of the
176 minor elements Mn, Mg and Ti, present at 0.1-0.3 wt% oxide). Solution nebulisation (SN) ICP-MS
177 trace element analyses were performed on a range of proximal and distal bulk cover-bed samples of
178 Lepu  Tephra including individual accretionary lapilli, and bulk samples from ODP core 1233D.
179 Approximately 0.25 g of sample was digested in hot open HF/HClO₄, after grinding in an agate
180 mortar and pestle, the solution made up to 250 mL in 2.5% HCl and analysed using an Agilent 7500
181 ICP-MS running in collision [He] mode. Analyses were performed alongside certified reference
182 materials JA-3 (andesite) and QLO-1 (quartz latite) (see GeoReM, 2014), which gave results accurate
183 to within $\pm 2\text{-}5\%$. Full details of analytical methods are given by Alloway et al. (2017a), which should
184 be consulted as the repository of compositional data used in this study. Major element data are
185 presented in Alloway et al. (2017a), and trace element data are presented in the supplementary
186 information to this paper, as well as Alloway et al. (2017a). X-ray diffraction (XRD) analyses were
187 conducted on a selection of bulk samples covering the fall-out of the Lepu  Tephra at the National
188 Museum of Wales, Cardiff, using a Panalytical X'Pert XRD with peak recognition and mineral
189 quantification achieved using Panalytical HighScore software, with a typical phase detection limit
190 between 0.1% and 1%.

191

192 **4. Mineralogy**

193 **Table 1 about here**

194 The results from XRD analysis of the bulk samples indicate that the majority of phenocrysts in the
195 Lepu  Tephra are plagioclase (plag., and fitted by the Panalytical HighScore software as a disordered
196 sodian anorthite composition - $[\text{Ca}_{0.83}, \text{Na}_{0.17}] (\text{Si}, \text{Al})_4 \text{O}_8$, from JCPDS File 00-041-1481), augite (aug.)
197 and quartz (qtz, see Table 1). The average bulk mineralogical composition of accretionary lapilli and
198 the bulk proximal Lepu  Tephra samples (<40 km from Volc n Michinmahuida) are extremely similar

199 (accretionary lapilli - 32% aug., 61% plag., 6% qtz, 1% titanomagnetite (Ti-Mt); bulk tephra - 30%
200 aug., 63% plag., 7% qtz). In the three distal tephra samples studied, there is a steady decrease in
201 augite content and a concomitant increase in plagioclase with increasing distance from Volcán
202 Michinmahuida. This mineralogical change coincides with a general thinning of the tephra and
203 increasing alteration, with a colour change to more red-brown hues related to the oxidation of Fe.
204 One accretionary lapillus has titanomagnetite recorded as a minor phase, and in the distal bulk
205 tephra sample at 80 km from Volcán Michinmahuida, magnetite is recorded, most likely associated
206 with weathering (hydration) of the tephra and oxidation of Fe²⁺-bearing phases.

207

208 **5. Compositional variation within the Lepu  tephra**

209 Alloway et al. (2017a) considered some aspects of the composition of the Lepu  Tephra, using major
210 element glass chemistry and a limited range of trace element data to show that this supported the
211 stratigraphic (field-based) correlation of the various Lepu  Tephra occurrences. However, it was
212 apparent from this earlier study that the data were not straightforward, with problems (for both
213 major and trace element single grain analyses) arising from the analysis of phenocrystic glass. The
214 glass component of shards from all analysed samples is rhyolitic (~71 wt % SiO₂) when free of
215 microphenocrysts, but when the shards contain numerous microlites, EPMA generates a basaltic-
216 andesite "bulk shard" composition with ~55 wt % SiO₂ as a mix of rhyolitic glass and abundant
217 phenocrysts (see Table 2 and Figures 18 and 19 in Alloway et al., 2017a). The pervasive alteration of
218 the tephra during weathering and soil-forming processes alters the glass phase so that only a limited
219 number of samples preserve material suitable for microbeam analysis, and has the potential to
220 change the composition of the tephra by adding or removing mobile elements from the deposit. For
221 these reasons Alloway et al. (2017a) in their tephra correlation study chose to provide only a limited
222 discussion of the tephra bulk compositional data. In the present paper, the single grain trace
223 element data (by LA-ICP-MS) are revisited, and compared with a fuller consideration of the bulk
224 sample trace element data to provide a robust geochemical correlation based on trace elements
225 which are both incompatible and immobile, and thus have inter-element ratios which (i) are immune
226 from the effects produced by incorporation of phenocrysts in microbeam analyses and (ii) remain
227 essentially unchanged during weathering. These elements form a subset of those high field strength
228 elements (e.g. Y, Zr, Nb, REE, Hf, Ta, Th, U) that are generally regarded to be (but do not always
229 behave as) both incompatible and immobile. The truly incompatible and immobile elements will be
230 shown to provide a means to correlate phenocryst-rich, deeply weathered tephra deposits such as
231 the Lepu  Tephra that are challenging from an analytical perspective.

232 **Figure 4 about here**

233 *5.1 Single grain trace element analyses*

234 Figure 4 shows a selection of LA-ICP-MS trace element data from analyses of single shards of the
235 Lepu  Tephra. The Sr-Zr data (Figures 4A, 4B) range from ~ 100 ppm to 1150 ppm Sr which
236 correlates with a steady decrease in Zr from around 650 ppm to ~25 ppm. This relationship relates to
237 an increasing proportion of phenocryst material (largely plagioclase) and a reduction in the amount
238 of glass ablated from the shard. Plagioclase feldspar has a high distribution coefficient (K_d) for Sr,
239 which substitutes readily for Ca, with K_d s in rhyolites and dacites ranging from 2.25-20, but has a low
240 K_d in augite ~0.5 (GERM, 2013). In contrast, Zr is incompatible in both plagioclase (K_d ~0.15) and
241 augite (K_d ~0.25). Incorporation of increasing amounts of a mixture of 2:1 plagioclase: augite in the
242 ablated material (proportions taken from XRD mineral abundances) will cause Sr to increase and Zr
243 to decrease compared to their concentrations in pure, microlite-free rhyolitic glass analyses (Pearce,
244 2014). The pure glass, which represents the frozen melt phase present at the time of eruption, forms
245 the cluster of analyses at <113 ppm Sr and between ~570-770 ppm Zr (see Figures 4A, 4B). Figure 4C
246 shows Zr-Y data. At the highest Zr concentrations (>~600 ppm Zr) analyses from all samples are
247 coincident and are of the pure glass phase, whereas in samples contaminated by the presence of
248 increasingly abundant phenocrysts (<~500 ppm Zr) the data spread out, with higher Y concentrations
249 in the more distal samples from ODP core 1233D and Lago Lepu . Yttrium is compatible in augite in
250 rhyolitic magmas (K_d s 2.6-7.6, GERM, 2013) and this spread in Y concentrations is likely to be the
251 result of the incorporation of higher quantities of augite in the ablated material. The difference from
252 the more proximal samples from Lago Paso Blanco, Puente Aguila and La Zeta, Esquel, may reflect
253 differences in the mineralogical composition of the magma (particularly the augite:plagioclase ratio)
254 from different phases of the eruption, particularly from the later eruption of less compositionally
255 evolved magma in a zoned magma body (see Alloway et al., 2017a). This behaviour is also shown by
256 the REE, where the middle (M)REE (e.g. Gd, Ho, Er) show similar behaviour to Y and are more
257 compatible in augite (Rollinson, 1993; GERM, 2013) than the light (L)REE (La, Ce) and heavy (H)REE
258 (Yb, Lu) which compare better with the more proximal samples. Figures 4D and 4E show data for Zr-
259 Th and Zr-Nb from single glass shards. Thorium and Nb, like Zr, are highly incompatible elements
260 with very low K_d s into plagioclase and augite, and because of this they show consistent ratios to Zr,
261 giving a tightly clustered array of data spreading from low concentrations where the analysed shard
262 contained abundant phenocrysts, to the pure glass (i.e. magmatic) composition at high Zr contents.
263 The consistency of these ratios, and equally the ratios of other incompatible elements in the glass
264 shards such as Hf, Ta, REE, and U, supports the correlation of all of these Lepu  Tephra samples.

265 **Figure 5 about here**

266 The dilution effect of the incorporation of phenocrystic material is also seen in chondrite-normalised
267 average REE data for all single shard analyses (Figure 5A). REE data from individual samples show
268 similar, parallel patterns and slopes, but average concentrations vary by a factor of about 2 because
269 of the dilution from phenocryst ablation. When only the low Sr (<113 ppm) analyses are averaged
270 (Figure 5B), these represent the composition of the pure (phenocryst-free) glass phase (i.e. the
271 quenched magma), which has a higher average REE concentration, and the separate samples show a
272 narrower compositional range. No analyses of Lepué Tephra glass from Lago Lepué and only two
273 analyses from ODP core 1233D have less than 113 ppm Sr, indicative of the high phenocryst contents
274 in these later erupted, more distal deposits (Alloway et al., 2017a), presumably sourced from a
275 deeper, less evolved portion of the magma body feeding the eruption. As well as higher overall REE,
276 these low-Sr glass analyses also show a deeper negative Eu anomaly than the average of all data, a
277 result of the preferential incorporation of Eu^{2+} into plagioclase (which is excluded from the low Sr
278 averages). These data also confirm the regional correlation of the Lepué Tephra, but are limited to a
279 few proximal sites and cores where fresh glass samples could be obtained: no fresh glass was
280 recovered from the highly weathered, thin distal deposits from, for example, Isla Grande de Chiloé.
281 To assess the correlation of these deposits, bulk analyses of proximal and distal deposits were
282 performed.

283 *5.2 Bulk sample and accretionary lapilli trace element analyses*

284 Figure 6 shows a selection of trace elements plotted against Zr from solution nebulisation ICP-MS
285 analyses of bulk tephra and individual accretionary lapilli from the Lepué Tephra, grouped according
286 to depositional distance from Volcán Michinmahuida. Other weathered tephra layers which are
287 stratigraphically associated with the Lepué Tephra, and from field evidence were interpreted to be
288 of a Volcán Michinmahuida source (e.g. Figure 2C) are plotted for comparison: they are not
289 correlatives of the Lepué Tephra, but nonetheless show similar compositional attributes (Alloway et
290 al., 2017a). Rubidium vs Zr (Figure 6A) show a very wide spread of the data, with the distal samples
291 showing low Rb at high Zr, although many of the proximal samples and accretionary lapilli are of
292 similar composition. Rubidium is a soluble and mobile alkali metal, and in the highly altered and
293 oxidised distal samples it is likely to have been removed in solution from the original tephra, while Zr
294 (insoluble) will not have been affected, remaining in the tephra as an immobile element. It is thus
295 possible that Zr may have been concentrated during the weathering of the tephra by the relative
296 loss in mass through dissolution by hydrolysis of original glass and mineral components, taking
297 soluble components such as the alkalis, Ca and Mg (as dissolved ions) and silica (as silicic acid) from
298 the tephra during weathering (Faure, 1998; Churchman and Lowe, 2012). This oxidative weathering
299 would leave a leached residue also relatively enriched in “insoluble” Al and Fe and Mn (Tardy and

300 Nahon, 1985). In contrast, two bulk samples of Lepu  Tephra from ODP core 1233D (core depths of
301 14.68 m and 14.80 m, each analysed in triplicate) shows Rb concentrations about twice the average
302 of proximal bulk and accretionary lapilli samples. The high Rb in the ODP 1233D core sample seems
303 most likely to result from the mixing of marine clays, generally rich in Rb (Li and Schoonmaker, 2003)
304 into the tephra layer by bioturbation and/or co-deposition (Todd et al., 2014). Because of this, the
305 analysis of a bulk sample of this marine occurrence of distal tephra (a mixture of tephra and marine
306 clay) is likely to not be fully representative of the deposit as a whole, but no samples of the enclosing
307 marine sediment were analysed in this study, and no sediment composition data from ODP core
308 1233D have been published. The individual glass shard chemistry (from unaltered glass, which is
309 frequently well-preserved in marine sediments) however clearly identifies it as Lepu  Tephra (see
310 above).

311 **Figure 6 about here**

312 Yttrium is plotted against Zr from bulk tephra analyses in Figure 6B and this, somewhat
313 unexpectedly, shows a wide spread of the Y compositions. More commonly Y would generally be
314 expected to show a good correlation with Zr showing a well-defined, consistent ratio (e.g. Pearce et
315 al., 2002; Alloway et al., 2015; Alloway et al., 2017b; Martin-Jones et al., 2017b). This is a result of Y
316 being generally both incompatible and immobile, although in some circumstances it can be
317 incorporated in some phenocryst phases, e.g. augite (with MREE, see above) and amphibole or
318 garnet at high pressure (e.g. Harangi et al., 2007), although these are not observed in the Lepu 
319 Tephra . Notably for the Lepu  Tephra, the distal cover-bed deposits show the lowest Y/Zr ratios (i.e.
320 lowest Y) whilst the proximal samples and accretionary lapilli are similar in composition, and this
321 behaviour is also seen with Rb (Figure 6A). This reduction in concentration of Y in distal deposits
322 suggests that it too has been mobilised during alteration of the tephra in this hyper-humid high-
323 weathering environment. Similar behaviour to Y is shown by all the REE, which also have the lowest
324 concentrations in the distal deposits (see data in Alloway et al., 2017a). Uranium (Figure 6C) shows a
325 moderate spread in concentrations and U/Zr ratio with the distal samples showing the lowest U/Zr
326 ratio but the distal samples do not show the marked depletion displayed by Y and the REE.

327 However U, like Rb, in the ODP 1233D core samples is about twice the concentration of proximal and
328 accretionary lapilli bulk analyses, and this is again consistent with mixing with marine sediments
329 which are generally relatively high in U (Li and Schoonmaker, 2003). This is particularly true if the
330 marine sediments are rich in organic material which promotes the reduction of the conservative
331 uranyl tricarbonate species present in oxic sea water causing the precipitation of uraninite (Pattan
332 and Pearce, 2009). OF the terrestrial deposits, the proximal Lepu  Tephra samples have the highest
333 U/Zr ratio, with lower U/Zr in distal samples and some accretionary lapilli, which is consistent with

334 oxidative weathering causing mobilisation of U. This is reflected in the general reddening of distal
335 deposits which results from the formation of insoluble Fe-oxides (presumably hematite, ferrihydrite,
336 or maghemite, e.g. Churchman and Lowe, 2012). Thorium and Nb are plotted against Zr in Figures 6D
337 and 6E, and show highly consistent ratios to Zr across the fall-out range, with no discernible
338 difference between proximal, distal or accretionary lapilli samples, apart from the higher Th in the
339 ODP 1233D samples, which can again be attributed to mixing with marine sediment where Th is
340 generally associated with the detrital clay fraction (Myers and Wignall, 1987). It is notable that both
341 Nb and Th are highest in the weathered, distal occurrences of the Lepué Tephra, again suggesting
342 their relative enrichment in insoluble phases (behaviour similar to Zr), resulting from the removal by
343 leaching of the more soluble components of the deposit, these “mobile” elements here including
344 REE, Y and U.

345 **Figure 7 about here**

346 The REE data from the bulk Lepué Tephra analyses are presented in Figure 7, averaged as groups
347 according to their occurrence or depositional distance from Volcán Michinmahuida. There is a clear
348 variation in the overall REE content of the samples with the highest concentrations shown by the
349 accretionary lapilli and the proximal samples, with low concentrations in ODP core sample 1233D
350 and in the distal samples. Modest negative Eu-anomalies are displayed in all samples, a result of the
351 extraction of feldspar during the evolution of the parent magma, and a distinct positive Ce-anomaly
352 is shown by the distal samples. The low concentrations in the ODP 1233D core sample may relate to
353 dilution of the primary tephra by marine sediment. In the distal samples, low REE concentrations are
354 related to mobility in these particular weathering conditions (*cf.* mobility of Y described above). In
355 contrast to the LA-ICP-MS glass data, the bulk sample REE data (Figure 7) do not show smooth
356 normalised curves (*cf.* Figure 5), but are more irregular displaying a series of evenly spaced “humps”
357 and intervening “cusps” with increasing atomic number. These features are most notable in the
358 proximal and distal terrestrial (cover-bed) samples and in the accretionary lapilli, with the cusps
359 between Nd-Pm, at Gd, and between Ho-Er, but these are not displayed by the ODP 1233D core
360 samples. This is a manifestation in the REE of the “tetrad effect” (Peppard, 1969; Bau, 1996) where
361 deviations from a smooth, steady change in REE behaviour related to ionic radius contraction occurs
362 to give cusped REE chondrite-normalised patterns. This behaviour, often referred to as non-CHARAC
363 – i.e. non-CHARGE-RADIUS Controlled (Bau, 1996) – results from the increased stability of REE ions at
364 quarter, half, three-quarter, and complete filling of the 4f electron shell and these effects have been
365 observed in a range of natural samples. Examples of the occurrence of tetrad effects in the REE
366 which may be relevant to the study of the weathered Lepué Tephra encompass magmatic processes
367 in granite magmas including late stage fractional crystallisation (Irber, 1999; Zhenhua et al., 2002);

368 extended groundwater interaction and alteration of granitic rocks (Masuda and Akagi, 1989;
369 Takahashi et al., 2002); co-precipitation of REE in Fe-Mn oxyhydroxides from solution (Bau, 1999;
370 Kawabe et al., 1999); processes occurring during argillic alteration (Abedini et al., 2018a) and the
371 formation of Ti-rich bauxites (Abedini et al., 2018b), and during chemical weathering associated
372 with the formation of *terre rosse* (Feng, 2010; Feng et al., 2011).

373 In the case of the Lepu  Tephra, the formation of a tetrad effect during any late-stage magmatic
374 processes can be excluded as the individual glass shard chemistry shows no signs of any tetrad or
375 non-CHARAC effects (see Figure 5B). The Lepu  Tephra displays “M-type” tetrad effects, where the
376 cusps form low points between convex-upward curved segments and this pattern has been
377 described in weathered materials with the opposite “W-type” curve being reported in groundwater
378 (Masuda and Ikeuchi, 1979; Masuda et al., 1987; Takahashi et al., 2002). The evidence indicates that
379 post-depositional terrestrial weathering in the soil-forming environment generated the observed
380 REE distributions within the Lepu  Tephra. This finding is further supported by consideration of REE
381 behaviour in Fe-oxyhydroxides that formed in the altered Lepu  Tephra to generate the red-orange
382 brown colouration. Secondary Fe-Mn oxyhydroxides formed during weathering or alteration
383 frequently display strongly developed tetrad effects (Bau, 1999; Kawabe et al., 1999; Feng, 2010;
384 Feng et al., 2011; Abedini et al., 2018b). In addition Fe-Mn oxyhydroxides, formed by precipitation
385 from oxidising waters, will also preferentially concentrate Ce^{4+} , the oxidised form of Ce, which can
386 lead to the generation of a positive Ce anomaly (Bau, 1999; Leybourne and Johannesson, 2008; Bau
387 and Koschinsky, 2009; Feng, 2010) as is observed in the distal cover-bed Lepu  Tephra deposits (see
388 Figure 7). The bulk sample REE data from ODP core 1233D shows neither any tetrad effect nor any
389 significant Ce anomaly, and again this indicates that these features in the cover-bed samples are not
390 primary magmatic features, but must be associated with surface, post-depositional processes which
391 do not affect the marine-deposited ODP core sample.

392 **Figure 8 about here**

393 Figure 8 shows the magnitude of any Ce anomaly (expressed as Ce/Ce^*) present in both the glass
394 analyses by LA-ICP-MS and the bulk sample analyses by SN-ICP-MS grouped by depositional distance
395 from Volc n Michinmahuida plotted against La (in ppm) from the Lepu  Tephra. The Ce anomaly is
396 calculated here by $Ce/Ce^* = 2\log Ce_N / (\log La_N + \log Pr_N)$ where Ce_N etc. represents the chondrite
397 normalised concentration. $Ce/Ce^* > 1$ indicates a positive Ce anomaly. The single glass shard analyses
398 show little or no Ce anomaly, clustering around $Ce/Ce^* \sim 1$, with La decreasing from about 60 ppm in
399 the pure glass phase (i.e. the magmatic composition) to a few ppm as increasing amounts of
400 phenocryst are incorporated in the analyses (La, and other REE are moderately to highly
401 incompatible in the major phenocryst phases in the Lepu  Tephra). In the bulk analyses of cover-bed

402 samples, however, it is clear that the magnitude of the Ce anomaly increases as the La concentration
403 decreases, with the majority of distally-deposited samples showing a marked positive Ce anomaly
404 (Ce/Ce^* up to ~ 1.5) and low La. This results from the leaching of trivalent REE (including La and Pr)
405 from the samples while Ce (present as Ce^{4+} in this oxidising weathering environment) is retained,
406 most likely to be sorbed on to an Fe-oxyhydroxide phase (Bau, 1999; Feng, 2010). Even some of the
407 thicker, proximal cover-bed deposits, and some accretionary lapilli show a reduction in La (and other
408 LREE) compared to a typical bulk composition of around 30 ppm, the reduced La and Pr generating
409 an increase in Ce/Ce^* , indicating that some of these samples also did not escape the ravages of this
410 oxidative chemical weathering.

411

412 **6. Chemical correlation of the Lepu  Tephra**

413 With only a limited number of samples from which fresh glass could be recovered for single grain
414 analyses, and the problems of extensive weathering noted in bulk sample analyses where mobility of
415 elements generally regarded as immobile such as the REE can be observed, it is appropriate to ask
416 whether geochemistry can be used to correlate the Lepu  Tephra across its entire fallout region.
417 The direct comparison of single-grain and bulk sample trace element analyses have been widely
418 cautioned against because of the problems of variable amounts of phenocryst incorporation in LA-
419 ICP-MS analyses, and the possibility for incorporation of non-juvenile material, alteration and/or
420 various sedimentary fractionation effects in bulk tephra analysis can complicate their interpretation
421 (Pearce et al., 2002; Pearce et al., 2007; Pearce et al., 2008; Pearce, 2014; Pearce et al., 2014;
422 Martin-Jones et al., 2017a). The Lepu  Tephra provides an excellent opportunity to test the use of
423 such data sets in correlation studies.

424 **Figure 9 about here**

425 Figure 9 compares selected bulk and single grain glass shard trace element data from all samples of
426 the Lepu  Tephra determined by either SN-ICP-MS or LA-ICP-MS. The concentrations of the
427 elements determined from the bulk samples are both lower and more limited in range than the glass
428 shard data, because the bulk samples are a mix of glass and mineral (maybe with or without lithics)
429 material whereas the single shard data records the range from the pure glass to almost entirely
430 mineral compositions (where microphenocrysts are abundant). However, for the highly incompatible
431 and immobile elements (Zr, Nb, Th, Hf, and Ta, Figures 9A-9C) inter-element ratios are identical for
432 the bulk samples and single shard analyses. For example, Zr/Th is 48.3 ± 8.7 in the bulk sample
433 analyses, and 47.1 ± 6.5 in the single shards, and Zr/Nb is 22.8 ± 4.5 in the bulk sample analyses, and
434 23.6 ± 3.2 in the single shards. These ratios therefore allow the comparison of bulk analyses with

435 single grain data, and confirm the correlation of the Lepu  Tephra across its fall-out despite using a
436 mix of data from different analytical methods. Although the Ta data shows a wider spread in LA-ICP-
437 MS data because of the lower instrument sensitivity (Pearce et al., 2004), the ratio Hf/Ta is also
438 indistinguishable between the two sets of data (i.e. bulk and single-grain analyses). In contrast,
439 Figures 9D-9F show the comparison for the two analytical methods for least one element per graph
440 which is mobile in the soil-forming environment (e.g. Sr, La, Rb, Cs), and it is clear that the single-
441 grain data cannot be compared with the bulk analyses for these mobile elements. Thus, while
442 limited confirmation of the correlation of the Lepu  Tephra was achieved using a few samples by
443 Alloway et al. (2017a), confirming the stratigraphic, field and morphological correlations, the
444 comparison here of element pairs from Zr, Hf, Nb, Ta, and U to give ratios, which are neither
445 influenced by the presence of phenocrysts in the ablated material, nor by weathering in the cover-
446 bed succession, provides a more robust method of correlation using this multi-method analytical
447 approach.

448 Incompatible trace element ratios from the Lepu  Tephra also differ from other Holocene tephra
449 deposits in the same region. The slightly younger Chana Tephra, *ca* 9750 cal a BP (Alloway et al.,
450 2017b), previously widely referred to as Cha-1, closely overlies the Lepu  Tephra at many sites and
451 has Zr/Nb of 8.4 ± 9 and Zr/Th of 5.6 ± 0.4 (162 LA-ICP-MS individual glass shard analyses), both
452 much lower and distinct from the Lepu  Tephra. Pumices from an early Holocene (~ 11.7 ka cal BP)
453 tephra deposit (RMV) erupted from the Volc n Mentolat, southern Chile, have Zr/Nb of 24.9 ± 3.7
454 and Zr/Th of 29.7 ± 3.7 (Weller et al., 2019), again different from the Lepu  Tephra. Three younger
455 (late Holocene) tephra deposits from Volc n Melimoyu have bulk sample (solution ICP-MS analyses)
456 Zr/Nb ratios of 18.2 ± 0.1 (Mm-1p), 18.1 ± 0.1 (Mm-1s) and 18.7 ± 0.6 (Mm-2), and Zr/Th ratios of
457 38.3 ± 0.2 (Mm-1p), 45.5 ± 0.5 (Mm-1s) and 34.8 ± 2.1 (Mm-2) (Geoffroy et al., 2018), and again the
458 ratios differ significantly from the Lepu  Tephra. Thus, these highly incompatible element ratios may
459 also serve to identify individual sources in the area, and allow discrimination between tephra
460 deposits. As yet, there are no data from the closely associated intensely weathered scoriaceous
461 lapilli tephra deposits from other local volcanoes which are likely to include Volc nes Corcovado,
462 Yate or Calbuco (see Figure 2C).

463

464 7. Conclusions

465 The elements Zr, Nb, Hf, Ta, and Th are highly incompatible in igneous systems, preferring to remain
466 in the magma rather than entering crystallising phases, even in relatively evolved rhyolitic magmas,
467 prior to the onset of zircon or other accessory phase crystallisation. This is the case for the $\sim 71\%$ SiO₂

468 magma (containing abundant phenocrysts to give an overall intermediate bulk-rock composition),
469 which erupted to form the Lepu  Tephra. Many other elements also behave incompatibly in rhyolitic
470 magmas (for example, the REE, Y, and U), but of the incompatible elements it is only Zr, Nb, Hf, Ta,
471 and Th, which remain immobile once exposed to weathering after deposition in the hyper-humid
472 andic soil-forming environment prevalent in this region of northern Patagonia/southern Chile. In
473 these hyper-humid, oxidising conditions the REE, Y and U become mobilised, with significant
474 fractionation of the REE occurring to leave weathered cover-bed tephra deposits with irregular
475 chondrite normalised REE patterns and positive Ce anomalies. These features result from the non-
476 CHARAC behaviour of the REE and the preferential sorption of Ce^{4+} onto secondary Fe-oxyhydroxides
477 precipitated as residual phases during the alteration of the tephra. The effects of this sub-aerial
478 oxidative weathering are most extensive on the thinner, more distal terrestrial tephra deposits, but
479 even some of the thicker, proximal deposits (which may be up to ~2 m thick) are not immune to the
480 compositional changes imparted by weathering, as observed in some of the accretionary lapilli bulk
481 sample analyses. The ODP 1233D core sample is, however, unaffected by weathering, but its bulk
482 composition would appear to include incorporated marine sediment relatively rich in U, Th and Rb,
483 which moves if away from the bulk analyses of the Lepu  Tephra. However, data from unaltered
484 glass shards within the tephra samples from ODP 1233D indicates this is clearly Lepu  Tephra.

485 For the terrestrial deposits of the Lepu  Tephra, only a few cover-bed samples yield glass shards
486 suitable for LA-ICP-MS trace element analysis, and intense weathering by hydrolysis and high rainfall
487 have resulted in the leaching of elements (solutes) from the bulk tephra making straightforward
488 comparisons of bulk analyses problematic. Because of this alteration and loss by leaching, chemical
489 correlation across the entirety of the tephra fall cannot easily be achieved by consideration of data
490 from only one analytical method. The consideration of a set of ratios for elements that are both
491 incompatible and immobile, however, allows data from bulk and single grain analytical methods to
492 be compared. For the fall-out region of the Lepu  Tephra, it is the ratios of Zr, Nb, Hf, Ta, and Th that
493 provide a basis for robust correlation and inter-method comparison, particularly when chemical
494 correlations are considered alongside detailed stratigraphic information. These elements are only a
495 subset of those elements generally considered to be immobile, a group which would typically also
496 include the REE, Y, and U. In considering the compositional data from the Lepu  Tephra, Alloway et
497 al. (2017a) concluded that "These results indicate the limited utility of bulk analyses in the absence
498 of associated chronostratigraphic contexts to be able to adequately differentiate [Volc n
499 Michinmahuida]-sourced eruptives". While there are certainly challenges in interpreting bulk
500 chemical data, particularly from such variably altered, intermediate tephra deposits, the careful
501 consideration of the data (as presented here) can allow reliable correlations to be made, which

502 substantiate the stratigraphic information, and can allow these bulk analyses to be linked in to the
503 single-grain glass shard chemistry. Consideration of Zr, Hf, Nb, Ta and Th in this high weathering
504 environment specifically overcomes the issue of element mobility (as displayed by the REE here),
505 and their incompatibility allows for robust inter-method comparisons. In the case of the Lepué
506 Tephra, the behaviour of the more mobile elements in this setting (e.g. the REE) from bulk sample
507 analysis also gives an indication of the conditions (i.e. oxidising) in which the weathering occurred.
508 Thus, in the most unpromising of analytical or geochemical conditions, ratios of the highly
509 incompatible and immobile elements (Zr, Hf, Nb, Ta, Th) enable the comparison of bulk and single
510 grain analyses, and provide a means for robust compositional tephra correlation, while the REE, Y, U
511 are mobilised by weathering in these hyper-humid soil-forming environments and must be regarded
512 accordingly. This approach using element ratio data from bulk and single grain analyses for immobile
513 incompatible elements has great potential in the study of weathered, phenocrystic tephra deposits.
514 This new approach is especially important in helping enable such variably weathered tephras to be
515 correlated over much great distances than previously attained, and hence their usefulness as
516 chronostratigraphic tools in multiple Quaternary-related studies is considerably enhanced.

517

518 **Acknowledgements**

519 This study was funded in part by grants from Aberystwyth University Research Fund to NJGP and a
520 Victoria University of Wellington Science Faculty Research Grant to BVA. Some fieldwork undertaken
521 by BVA was also funded by Iniciativa Científica Milenio grants P02-51 and NC120066, Fondecyt
522 1151469 to Patricio Moreno, Universidad de Chile, Santiago. Richard Bevins and Tom Cotterell at the
523 National Museum of Wales, Cardiff, are thanked for assisting NJGP with the XRD analyses and
524 providing facilities during a period of research leave. At Aberystwyth University, Andy Brown at
525 DGES, is thanked for assisting with/conducting solution-ICP-MS analyses and Ron Fuge is thanked for
526 his comments on an earlier draft of this manuscript. We would like to thank the two QI referees
527 (David Lowe, University of Waikato and anonymous) for their comments, and also Andrei Sarna-
528 Wojcicki, USGS, for his additional and insightful comments, all of which have helped clarify and
529 improve this contribution.

530 **Tables**

531

532 **Table 1.** Mineralogical abundances (%) in samples of Lepué Tephra measured by X-ray diffraction.

533 “Na-An” is a plagioclase of sodian anorthite composition from JCPDS Data File 00-041-1481.

534 Distances measured as straight line from the top of Volcán Michinmahuida. Abbreviations: Qtz-

535 quartz; Ti-Mt – titanomagnetite; Mt – magnetite. Other phases identified as present in the Lepué

536 Tephra are listed, but these are <~1%, and in some cases these more exotic mineral species are likely

537 to be an artefact of the software peak fitting at such low abundances. Nanocrystalline minerals,

538 namely allophane and ferrihydrite, together with hydrous Fe-oxides (e.g. haematite) are likely to be

539 present in these andic soils (Churchman and Lowe, 2012), but will not be specifically identified by

540 XRD in this study.

541

Sample	Dist. km	Aug.	Na-An	Qtz	Ti-Mt	Mt	Other phases reported at trace amounts (treat identification with caution)
Proximal							
Pum 4-1	18	22	71	7			Tremolite, leifite
S5.1	22.5	37	56	6			
15J13S9C	31	29	65	6			
11J13S12-T2	38	33	60	8			Broad clay “peak” at 10° 2θ
Distal							
9J13S5-T1	80	35	57	6		3	
8J13S2-T1	120	23	73	4			Leifite, eckermannite, rouvillite (carbonate)
Chapo Rd S1-1	144	0	94	6			Humite, pigeonite?
Accretionary lapilli (proximal)							
S8.3 (5)	25	25	68	7			Nimesite (clay kaolinite-serpentinite group)
S9.1 (13)	29	30	64	1	4		
S13.1 (1)	38.5	31	59	10			
Cor-1 S1 (2)	41	41	53	6			Lizardite (clay kaolinite-serpentinite group)

542

543 **Figures – submitted as 2400 dpi eps files**

544 **Figure 1.** Map of the study area indicating the distribution and sample locations of the Lepué Tephra.
 545 Open red circles are lake cores occurrences, open green diamonds are thin (typically <10 cm) tephra
 546 samples from cover-bed sequences referred to as “distal” from Volcán Michinmahuida, and open
 547 blue squares are thicker tephra samples (>> 30 cm) from cover-bed sequences “proximal” to Volcán
 548 Michinmahuida. ODP sites 1233D is marked where a 12 cm thick layer of Lepué Tephra is recorded.
 549 Dashed ellipse marks the 1 cm isopach, and is the approximate extent of Lepué Tephra in visible in
 550 cover-bed sequences. Thickness data for individual occurrences, locality information and
 551 stratigraphic logs can be obtained from Alloway et al. (2017a). Abbreviations: **L. Ll.** – Lago
 552 Llanquihue, **V. Mm.** – Volcán Melimoyu (see Geoffroy et al., 2018), **V. Ch.** – Volcán Chaiten (see
 553 Alloway et al., 2017b), **V. Co.** – Volcán Corcovado.

554 **Figure 2.** The range of field occurrences of Lepué Tephra throughout northwest Patagonia. For
 555 locality and stratigraphic information pertaining to each site see Alloway et al. (2017a). **A.** Proximal
 556 occurrence just north of Chaitén (Section 8, 17 km west of Volcán Michinmahuida). Lower arrow
 557 indicates the weathered scoriaceous orange lapilli-rich basal layer (magmatic phase) of Lepué
 558 Tephra eruption, whereas the upper arrow indicates the grey poorly sorted massive to weakly
 559 stratified scoriaceous ash layer (phreatomagmatic phase). **B.** Accretionary lapilli in proximal deposit
 560 from Section 8, the largest here are ~2.5 cm in diameter. **C.** Massive grey Lepué Tephra (arrowed)
 561 (Section 1, 40 km south of Volcán Michinmahuida) enveloped by strongly weathered orange-
 562 coloured pumice-lapilli rich tephra beds and andic soil interbeds. Spade (marked) for scale (~1m
 563 long) resting on lower bedrock exposure. **D.** Distal Lepué Tephra, 12 cm thick, from La Paloma, 170
 564 km NNW of Volcán Michinmahuida, just north of Puerto Montt. **E.** Lepué Tephra forming
 565 discontinuous cemented ash pods overlying glacial deposits at Queilen, Isla Grande de Chiloé, 85 km
 566 west of Volcán Michinmahuida. **F.** Lepué Tephra forming subtle discontinuous cemented ash pods ~
 567 3 cm in diameter (inclined arrows), approximately 30 cm below the diffuse white rhyolitic distal 9.7
 568 ka Chana Tephra (between upper horizontal arrows, formerly Cha-1, see Alloway et al., 2017b) at the
 569 Cholgo section, 85 km north of Volcán Michinmahuida. This is Section A of Watt et al. (2011), but
 570 they do not record the occurrence of any tephra below the Chana Tephra. Knife is 20 cm long.

571 **Figure 3.** Back scattered electron images of individual glass shards from the Lepué Tephra, showing
 572 the range of microlite contents and vesicularity in pairs of shards from three samples: **A-B** – Lago
 573 Lepué, Chiloé (distal); **C-D** – ODP core 1233D (distal); **D-E** – Puente Aguila Road Section 5, ~20 km
 574 NNW of Volcán Michinmahuida (proximal) (see Figure 1 and Alloway et al., 2017a). In each case low
 575 microlite contents are illustrated on the upper row (**A, C, E**) and high microlite contents on the lower
 576 row (**B, D, F**). Note different scale bars for different images of either 10 μm (**A, C, D**) or 100 μm (**B, E, F**).
 577 In microlite rich samples (and some samples with relatively “low” microlite contents), it is
 578 impossible to place a 20 μm diameter LA-ICP-MS analysis without ablating phenocrystic material.

579 **Figure 4.** Plots of selected trace element concentrations for single glass shard analyses determined
 580 by LA-ICP-MS. See text for discussion. All concentrations in ppm.

581 **Figure 5. A.** Plot of chondrite-normalised average composition of REE for all single shard analyses of
 582 samples analysed by LA-ICP-MS. **B.** Plot of chondrite-normalised average composition of REE for
 583 samples analysed by LA-ICP-MS with <113 ppm Sr, i.e. those analyses of “pure” glass, free from the
 584 ablation of phenocrystic material. Note no samples from Lago Lepué have less than 113 ppm Sr. See
 585 text for discussion. Chondrite compositions from Sun and McDonough (1989).

586

587 **Figure 6.** Plots of selected trace elements against Zr for solution nebulisation ICP-MS analyses of bulk
588 tephra and individual accretionary lapilli from the Lepué Tephra. Analyses are grouped according to
589 depositional distance from Volcán Michinmahuida (see Figure 1). “Associated tephra” indicates
590 other weathered tephra layers stratigraphically associated with the Lepué Tephra (see for example
591 Figure 2C) and, based on field evidence, were initially interpreted to be of a Volcán Michinmahuida
592 source (Alloway et al., 2017a). All concentrations in ppm.

593 **Figure 7.** Chondrite-normalised average composition of REE for grouped Lepué Tephra deposits,
594 analysed by SN-ICP-MS. Some groups show the presence of “M-type” tetrad effects, notably
595 between Gd and Lu in proximal, distal and accretionary lapilli samples (note the relatively high
596 concentrations of Tb and Tm-Yb compared to neighbouring REE). Arrows mark the boundaries
597 between the four individual tetrads which include La-Nd, Sm-Gd, Gd-Ho and Er-Lu. The second
598 tetrad (Sm-Eu) is often unclear as it includes Eu, which shows variable oxidation states leading to the
599 common occurrence of anomalous behaviour in magmatic systems, and should include Pm, the
600 highly radioactive REE which is no longer present at the Earth’s surface. See text for discussion.
601 Chondrite compositions from Sun and McDonough (1989).

602 **Figure 8.** The magnitude of any Ce anomaly (expressed as Ce/Ce^* where values >1 indicate a positive
603 Ce anomaly) compared to La concentration (in ppm) from the Lepué Tephra from both LA-ICP-MS
604 analyses of single glass shards, and bulk analysis of samples by SN-ICP-MS, grouped by depositional
605 distance/setting from Volcán Michinmahuida.

606 **Figure 9.** Comparison of selected trace element data from the Lepué Tephra determined by either
607 LA-ICP-MS or SN-ICP-MS. For the highly incompatible and highly immobile elements (Zr, Nb, Hf, Ta,
608 Th) element ratios are identical for the two methods applied and provide a means for correlation. All
609 concentrations in ppm.

610

611 **References**

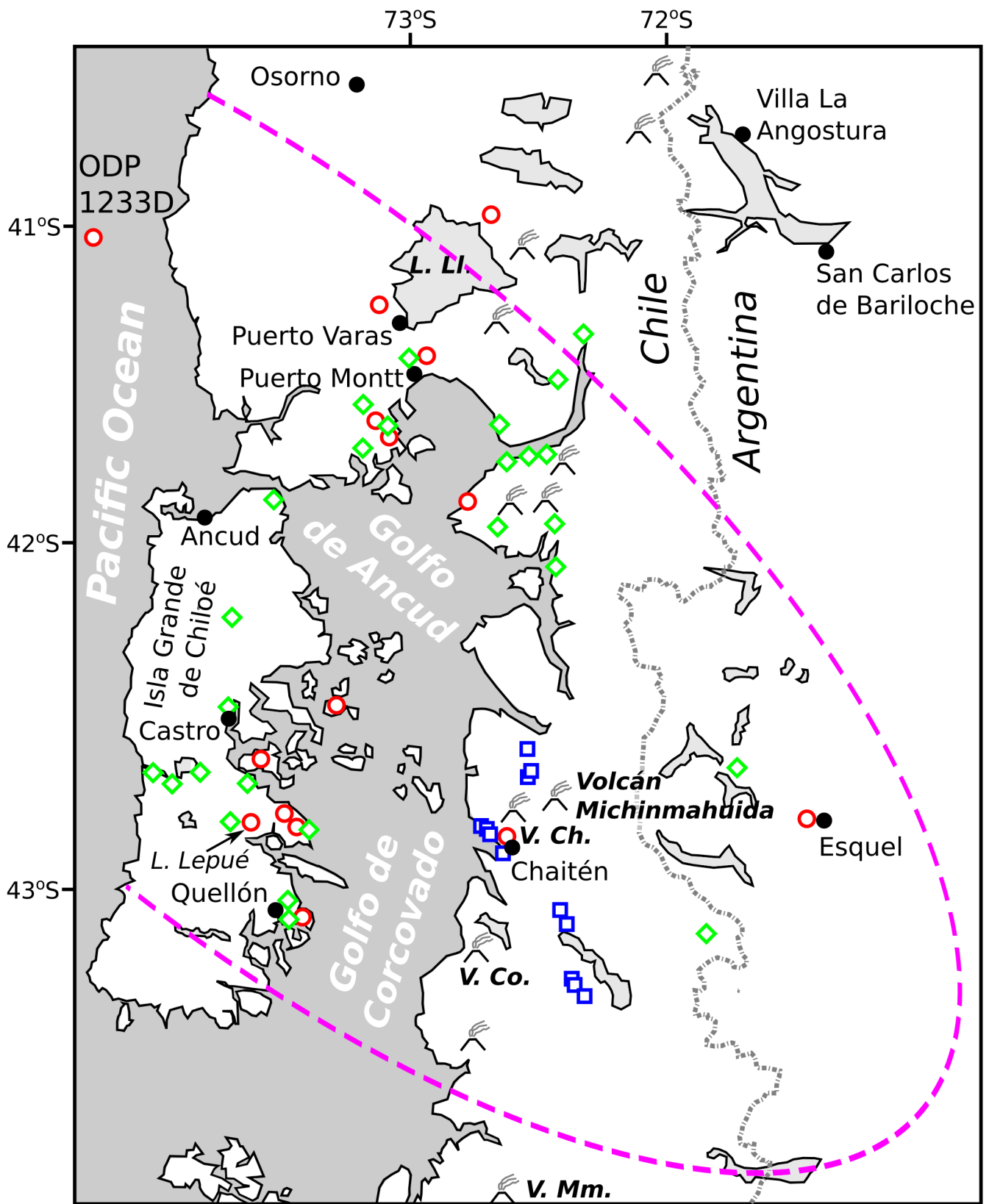
- 612 Abbott, P.M., Austin, W.E.N., Davies, S.M., Pearce, N.J.G., Hibbert, F.D., 2013.
613 Cryptotephrochronology of a North East Atlantic marine sequence over Termination II, the
614 Eemian and the last interglacial-glacial transition. *Journal of Quaternary Science*, 28: 501-
615 514.
- 616 Abedini, A., Azizi, M.R., Calagari, A.A., 2018a. The Lanthanide Tetrad Effect in Argillic Alteration: An
617 Example from the Jizvan District, Northern Iran. *Acta Geologica Sinica*, 92: 1468-1485.
- 618 Abedini, A., Calagari, A.A., Azizi, M.R., 2018b. The tetrad-effect in rare earth elements distribution
619 patterns of titanium-rich bauxites: Evidence from the Kanigorgeh deposit, NW Iran. *Journal*
620 *of Geochemical Exploration*, 186: 129-142.
- 621 Alloway, B., Neall, V., Vucetich, C., 1995. Late Quaternary (post 28,000 year BP) tephrostratigraphy
622 of northeast and central Taranaki, New Zealand. *Journal of the Royal Society of New*
623 *Zealand*, 25(4): 385-458.
- 624 Alloway, B.V., Moreno, P.I., Pearce, N.J.G., De Pol-Holz, R., Henriquez, W.I., Pesce, O.H., Sagredo, E.,
625 Villarosa, G., Outes, V., 2017a. Stratigraphy, age and correlation of Lepu  Tephra: a
626 widespread c. 11,000 cal. A BP marker horizon sourced from the Chait n Sector of southern
627 Chile. *Journal of Quaternary Science*, 36: 795-829.
- 628 Alloway, B.V., Pearce, N.J.G., Moreno, P.I., Villarosa, G., Jara, I., De Pol-Holz, R., Outes, V., 2017b. An
629 18,000 year-long eruptive record from Volc n Chait n, northwestern Patagonia:
630 Paleoenvironmental and hazard-assessment implications. *Quaternary Science Reviews*, 168:
631 151-181.
- 632 Alloway, B.V., Pearce, N.J.G., Villarosa, G., Outes, V., Moreno, P.I., 2015. Multiple melt bodies fed the
633 AD 2011 eruption of Puyehue-Cord n Caulle, Chile. *Scientific Reports*, 5.
- 634 Bau, M., 1996. Controls on the fractionation of isoivalent trace elements in magmatic and aqueous
635 systems: evidence from Y/Ho, Zr/Hf, and lanthanide tetrad effect. *Contributions to*
636 *Mineralogy and Petrology*, 123(3): 323-333.
- 637 Bau, M., 1999. Scavenging of dissolved yttrium and rare earths by precipitating iron oxyhydroxide:
638 experimental evidence for Ce oxidation, Y-Ho fractionation, and lanthanide tetrad effect.
639 *Geochimica et Cosmochimica Acta*, 63(1): 67-77.
- 640 Bau, M., Koschinsky, A., 2009. Oxidative scavenging of cerium on hydrous Fe oxide: evidence from
641 the distribution of rare earth elements and yttrium between Fe oxides and Mn oxides in
642 hydrogenetic ferromanganese crusts. *Geochemical Journal*, 43(1): 37-47.
- 643 Cas, R.A.F., Wright, J.V., 1987. *Volcanic successions*. Chapman and Hall, London, 528 pp.
- 644 Churchman, G.J., Lowe, D.J., 2012. Alteration, formation, and occurrence of minerals in soils. In:
645 Huang, P.M., Li, Y., Sumner, M.E. (Eds.), *Handbook of Soil Sciences*. 2nd edition. Vol. 1:
646 *Properties and Processes*. CRC Press (Taylor and Francis), Boca Raton, FL, pp. 20.1-20.72.
- 647 Cronin, S.J., Neall, V.E., Stewart, R.B., Palmer, A.S., 1996. A multiple-parameter approach to andesitic
648 tephra correlation, Ruapehu volcano, New Zealand. *Journal of Volcanology and Geothermal*
649 *Research*, 72(3-4): 199-215.
- 650 Donoghue, S.L., Vallance, J., Smith, I.E., Stewart, R.B., 2007. Using geochemistry as a tool for
651 correlating proximal andesitic tephra: case studies from Mt Rainier (USA) and Mt Ruapehu
652 (New Zealand). *Journal of Quaternary Science: Published for the Quaternary Research*
653 *Association*, 22(4): 395-410.
- 654 Faure, G., 1998. *Principles and applications of geochemistry: a comprehensive textbook for geology*
655 *students*. Prentice Hall, New Jersey, 600 pp.
- 656 Feng, J.-L., 2010. Behaviour of rare earth elements and yttrium in ferromanganese concretions,
657 gibbsite spots, and the surrounding terra rossa over dolomite during chemical weathering.
658 *Chemical Geology*, 271(3-4): 112-132.
- 659 Feng, J.-L., Gao, S.-P., Zhang, J.-F., 2011. Lanthanide tetrad effect in ferromanganese concretions and
660 terra rossa overlying dolomite during weathering. *Chemie der Erde-Geochemistry*, 71: 349-
661 362.

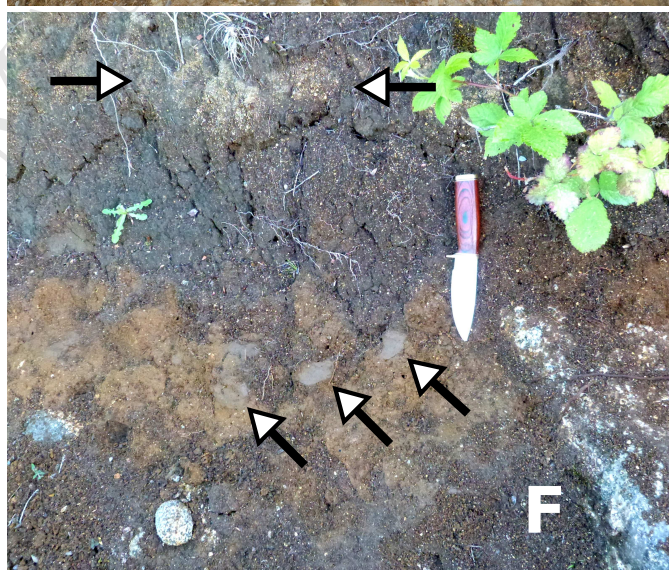
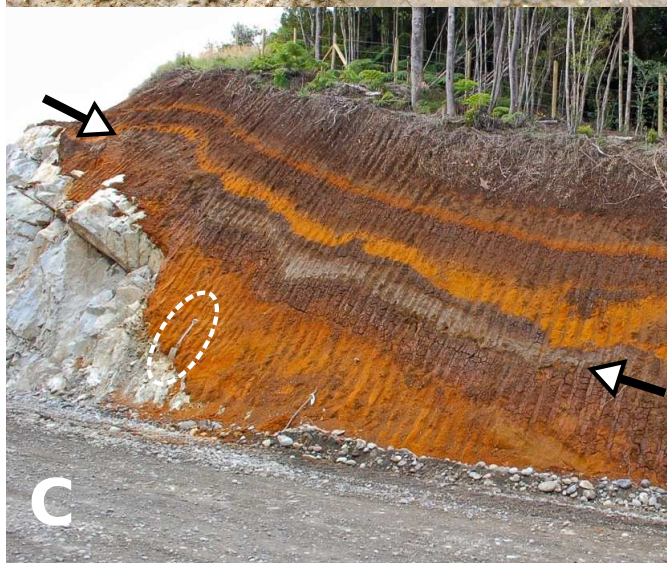
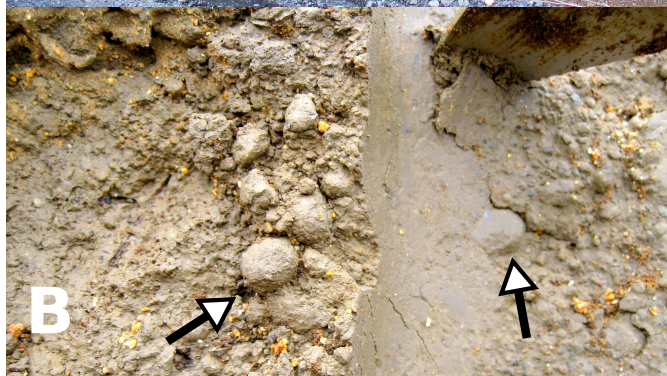
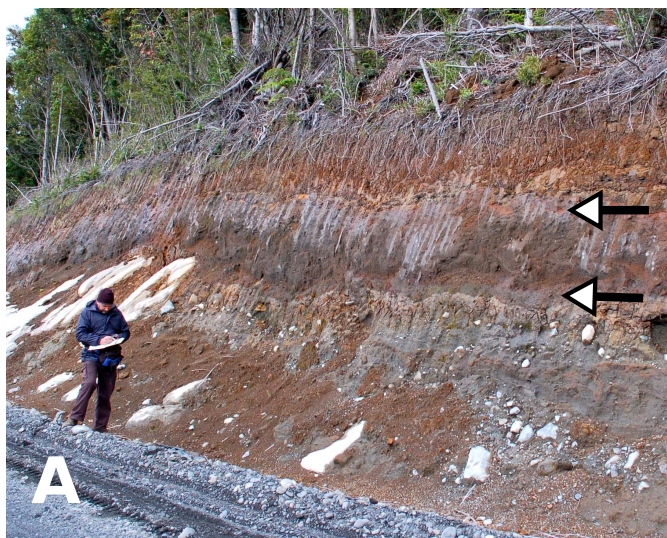
- 662 Geoffroy, C., Alloway, B.V., Amigo, À., Parada, M., Gutierrez, F., Castruccio, A., Pearce, N.J., Morgado,
663 E., Moreno, P., 2018. A widespread compositionally bimodal tephra sourced from Volcán
664 Melimoyu (44° S, Northern Patagonian Andes): Insights into magmatic reservoir processes
665 and opportunities for regional correlation. *Quaternary Science Reviews*, 200: 141-159.
- 666 GeoReM, 2014. http://georem.mpch-mainz.gwdg.de/sample_query.asp.
- 667 GERM, 2013. Geochemical Earth Reference Model (GERM) Partition Coefficient (Kd) Database,
668 www.earthref.org/KDD/.
- 669 Gilbert, J.S., Lane, S., 1994. The origin of accretionary lapilli. *Bulletin of Volcanology*, 56(5): 398-411.
- 670 Harangi, S., Downes, H., Thirlwall, M., Gméling, K., 2007. Geochemistry, petrogenesis and
671 geodynamic relationships of Miocene calc-alkaline volcanic rocks in the Western Carpathian
672 arc, eastern central Europe. *Journal of Petrology*, 48(12): 2261-2287.
- 673 Irber, W., 1999. The lanthanide tetrad effect and its correlation with K/Rb, Eu/Eu*, Sr/Eu, Y/Ho, and
674 Zr/Hf of evolving peraluminous granite suites. *Geochimica et Cosmochimica Acta*, 63(3-4):
675 489-508.
- 676 Jochum, K.P., Stoll, B., Herwig, K., others, 2006. MPI-DING reference glasses for in situ microanalysis:
677 New reference values for element concentrations and isotope ratios. *Geochemistry,*
678 *Geophysics, Geosystems*, 7: Q02008, doi:10.1029/2005GC001060.
- 679 Juvigné, É., Porter, S.C., 1985. Mineralogical variations within two widespread Holocene tephra
680 layers from Cascade Range Volcanoes, USA. *Géographie physique et Quaternaire*, 39(1): 7-
681 12.
- 682 Kawabe, I., Ohta, A., Ishii, S., Tokumura, M., Miyauchi, K., 1999. REE partitioning between Fe-Mn
683 oxyhydroxide precipitates and weakly acid NaCl solutions: Convex tetrad effect and
684 fractionation of Y and Sc from heavy lanthanides. *Geochemical Journal*, 33(3): 167-179.
- 685 Kirkman, J., McHardy, W., 1980. A comparative study of the morphology, chemical composition and
686 weathering of rhyolitic and andesitic glass. *Clay minerals*, 15(2): 165-173.
- 687 Leybourne, M.I., Johannesson, K.H., 2008. Rare earth elements (REE) and yttrium in stream waters,
688 stream sediments, and Fe–Mn oxyhydroxides: fractionation, speciation, and controls over
689 REE+ Y patterns in the surface environment. *Geochimica et Cosmochimica Acta*, 72(24):
690 5962-5983.
- 691 Li, Y., Schoonmaker, J., 2003. Chemical composition and mineralogy of marine sediments, *Treatise of*
692 *Geochemistry*. Elsevier, pp. 1-35.
- 693 Lowe, D.J., 2011. Tephrochronology and its application: a review. *Quaternary Geochronology*, 6: 107-
694 153.
- 695 Lowe, D.J., Pearce, N.J.G., Jorgensen, M.A., Kuehn, S.C., Tryon, C.A., Hayward, C., 2017. Correlating
696 tephtras and cryptotephtras using glass compositional analyses and numerical and statistical
697 methods: review and evaluation *Quaternary Science Reviews*, 175: 1-44.
- 698 Lowe, D.J., Shane, P.A., Alloway, B.V., Newnham, R.M., 2008. Fingerprints and age models for
699 widespread New Zealand tephra marker beds erupted since 30,000 years ago: a framework
700 for NZ-INTIMATE. *Quaternary Science Reviews*, 27(1-2): 95-126.
- 701 Martin-Jones, C.M., Lane, C.S., Pearce, N.J.G., Smith, V.C., Lamb, H.F., 2017a. Recurrent explosive
702 eruptions from a high-risk Main Ethiopian Rift volcano throughout the Holocene. *Geology*.
- 703 Martin-Jones, C.M., Lane, C.S., Pearce, N.J.G., Smith, V.C., Lamb, H.F., Oppenheimer, C., Asrat, A.,
704 Schaebitz, F., 2017b. Glass compositions and tempo of post-17 ka eruptions from the Afar
705 Triangle recorded in sediments from Lake Ashenge and Lake Hayk, Ethiopia. *Quaternary*
706 *Geochronology*, 37: 15-31.
- 707 Masuda, A., Akagi, T., 1989. Lanthanide tetrad effect observed in leucogranites from China.
708 *Geochemical Journal*, 23(5): 245-253.
- 709 Masuda, A., Ikeuchi, Y., 1979. Lanthanide tetrad effect observed in marine environment.
710 *Geochemical Journal*, 13(1): 19-22.
- 711 Masuda, A., Kawakami, O., Dohmoto, Y., Takenaka, T., 1987. Lanthanide tetrad effects in nature: two
712 mutually opposite types, W and M. *Geochemical Journal*, 21(3): 119-124.

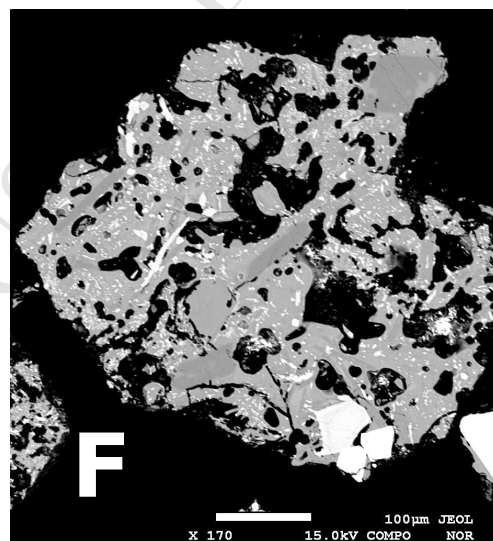
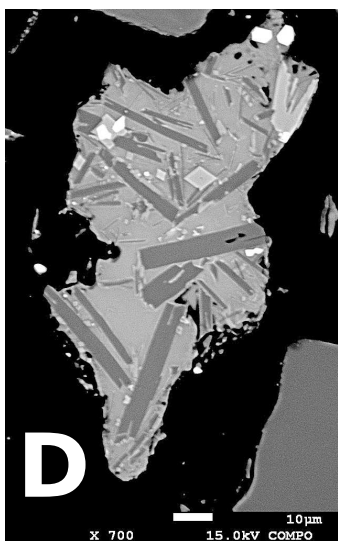
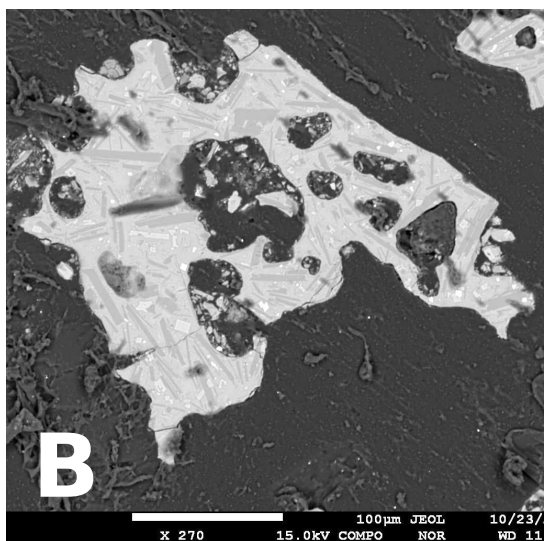
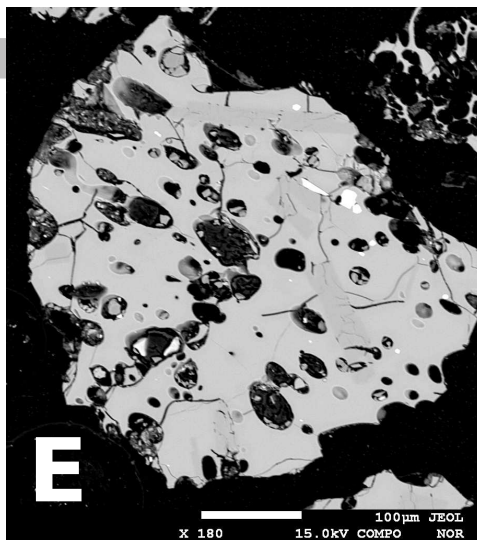
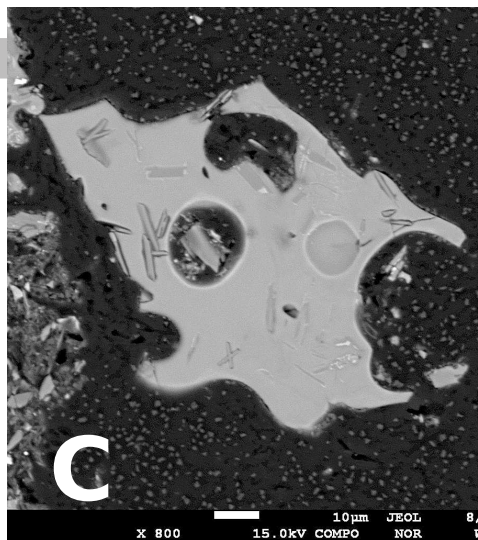
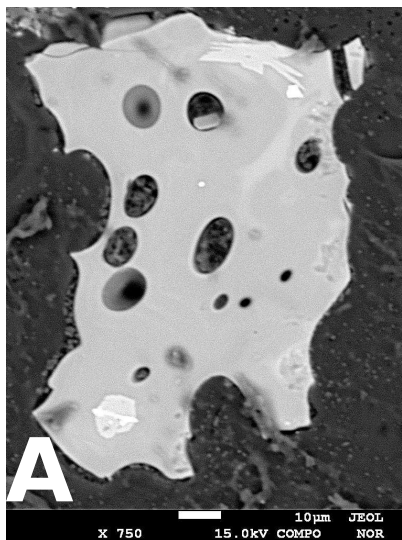
- 713 McHenry, L.J., Mollel, G.F., Swisher III, C.C., 2008. Compositional and textural correlations between
714 Olduvai Gorge Bed I tephra and volcanic sources in the Ngorongoro Volcanic Highlands,
715 Tanzania. *Quaternary International*, 178(1): 306-319.
- 716 Moore, J.G., Peck, D.L., 1962. Accretionary lapilli in volcanic rocks of the western continental United
717 States. *The Journal of Geology*, 70(2): 182-193.
- 718 Myers, K.J., Wignall, P.B., 1987. Understanding Jurassic organic-rich mudrocks—new concepts using
719 gamma-ray spectrometry and palaeoecology: examples from the Kimmeridge Clay of Dorset
720 and the Jet Rock of Yorkshire, *Marine clastic sedimentology*. Springer, pp. 172-189.
- 721 Naranjo, J.A., Stern, C.R., 2004. Holocene tephrochronology of the southernmost part (42°30'-45° S)
722 of the Andean Southern Volcanic Zone. *Revista geológica de Chile*, 31(2): 224-240.
- 723 Parfitt, R., Russell, M., Orbell, G., 1983. Weathering sequence of soils from volcanic ash involving
724 allophane and halloysite, New Zealand. *Geoderma*, 29(1): 41-57.
- 725 Pattan, J.N., Pearce, N.J.G., 2009. Bottom water oxygenation history in southeastern Arabian Sea
726 during the past 140 ka: Results from redox-sensitive elements. *Palaeogeography,*
727 *Palaeoclimatology, Palaeoecology*, 280: 396-405.
- 728 Pearce, N.J.G., 2014. Towards a protocol for the trace element analyses of glass from rhyolitic shards
729 in tephra deposits by laser ablation ICP-MS. *Journal of Quaternary Science*, 29: 627-640.
- 730 Pearce, N.J.G., Abbott, P.M., Martin-Jones, C., 2014. Microbeam methods for the analysis of glass in
731 fine grained tephra deposits: a SMART perspective on current and future trends. In: Austin,
732 W.E.N., Abbott, P.M., Davies, S.M., Pearce, N.J.G., Wastegard, S. (Eds.), *Marine*
733 *Tephrochronology*. Geological Society Special Publication, London.
- 734 Pearce, N.J.G., Bendall, C.A., Westgate, J.A., 2008. Comment on “Some numerical considerations in
735 the geochemical analysis of distal microtephra” by A.M. Pollard, S.P.E. Blockley and C.S.
736 Lane. *Applied Geochemistry*, 23: 1353-1364.
- 737 Pearce, N.J.G., Denton, J.S., Perkins, W.T., Westgate, J.A., Alloway, B.V., 2007. Correlation and
738 characterisation of individual glass shards from tephra deposits using trace element laser
739 ablation ICP-MS analyses: current status and future potential. *Journal of Quaternary Science*,
740 22: 721-236.
- 741 Pearce, N.J.G., Eastwood, W.J., Westgate, J.A., Perkins, W.T., 2002. The composition of juvenile
742 volcanic glass from the c. 3,600 B.P. Minoan eruption of Santorini (Thera). *Journal of the*
743 *Geological Society*, 159: 545-556.
- 744 Pearce, N.J.G., Perkins, W.T., Westgate, J.A., Gorton, M.P., Jackson, S.E., Neal, C.R., Chenery, S.P.,
745 1997. A compilation of new and published major and trace element data for NIST SRM 610
746 and NIST SRM 612 glass reference materials. *Geostandards Newsletter*, 21: 115-144.
- 747 Pearce, N.J.G., Perkins, W.T., Westgate, J.A., Wade, S.C., 2011. Trace element analysis by laser
748 ablation ICP-MS: the quest for comprehensive chemical characterisation of single sub-10µm
749 volcanic glass shards. *Quaternary International*, 246: 57-81.
- 750 Pearce, N.J.G., Westgate, J.A., Perkins, W.T., Preece, S.J., 2004. The application of ICP-MS methods to
751 tephrochronological problems. *Applied Geochemistry*, 19: 289-322.
- 752 Peppard, D., 1969. A tetrad effect in the liquid-liquid extraction ordering of lanthanides (III). *J. inorg.*
753 *nucl. Chem.*, 31: 2271-2272.
- 754 Platz, T., Cronin, S.J., Smith, I.E.M., Turner, M.B., Stewart, R.B., 2007. Improving the reliability of
755 microprobe-based analyses of andesitic glasses for tephra correlation. *The Holocene*, 17:
756 573-583.
- 757 Riehle, J.R., Miyaoka, R.T., Meyer, C.E., 1999. Data on Holocene tephra (volcanic ash) deposits in the
758 Alaska Peninsula and lower Cook Inlet region of the Aleutian volcanic arc, Alaska. USGS.
- 759 Rollinson, H.R., 1993. *Using Geochemical Data: Evaluation, Presentation, Interpretation*. Longman
760 Scientific and Technical Harlow, 376 pp.
- 761 Sarna-Wojcicki, A.M., Meyer, C.E., Woodward, M.J., Lamothe, P.J., 1981. Composition of air-fall ash
762 erupted on May 18, May 25, June 12, July 22 and August 7. In: Lipman, P.W., Mullineaux,

- 763 D.R. (Eds.), The 1980 eruptions of Mount St. Helens, Washington. United States Geological
764 Survey Professional Paper 1250.
- 765 Shane, P., 2005. Towards a comprehensive distal andesitic tephrostratigraphic framework for New
766 Zealand based on eruptions from Egmont volcano. *Journal of Quaternary Science*, 20(1): 45-
767 57.
- 768 Sun, S.-s., McDonough, W.F., 1989. Chemical and isotopic systematics of oceanic basalts:
769 implications for mantle compositions and processes. In: Saunders, A.D., Norry, M.J. (Eds.),
770 *Magmatism in the Ocean Basins*. Geological Society Special Publication, pp. 313-345.
- 771 Takahashi, Y., Yoshida, H., Sato, N., Hama, K., Yusa, Y., Shimizu, H., 2002. W-and M-type tetrad
772 effects in REE patterns for water–rock systems in the Tono uranium deposit, central Japan.
773 *Chemical Geology*, 184(3-4): 311-335.
- 774 Tardy, Y., Nahon, D., 1985. Geochemistry of laterites, stability of Al-goethite, Al-hematite, and Fe³⁺-
775 kaolinite in bauxites and ferricretes: an approach to the mechanism of concretion formation.
776 *American Journal of Science*, 285(10): 865.
- 777 Tiedemann, R., Mix, A.C., Richter, C., Ruddiman, W.F., 2007. Proceedings of the Ocean Drilling
778 Program. Scientific Results Leg 202. , Ocean Drilling Program, College Station, Texas.
- 779 Todd, J.A., Austin, W.E., Abbott, P.M., 2014. Quantifying bioturbation of a simulated ash fall event.
780 In: Austin, W.E., Abbott, P.M., Davies, S.M., Pearce, N.J.G., Wastegård, S. (Eds.), *Marine*
781 *Tephrochronology* Geological Society, London, pp. 195-207.
- 782 Watt, S.F., Pyle, D.M., Naranjo, J.A., Rosqvist, G., Mella, M., Mather, T.A., Moreno, H., 2011.
783 Holocene tephrochronology of the Hualaihue region (Andean southern volcanic zone, ~ 42
784 S), southern Chile. *Quaternary International*, 246(1-2): 324-343.
- 785 Weller, D., de Porras, M., Maldonado, A., Méndez, C., Stern, C., 2019. Petrology, geochemistry, and
786 correlation of tephra deposits from a large early-Holocene eruption of Mentolat volcano,
787 southern Chile. *Journal of South American Earth Sciences*, 90: 282-295.
- 788 Zhenhua, Z., Xiaolin, X., Xiaodong, H., Yixian, W., Qiang, W., Zhiwei, B., Jahn, B., 2002. Controls on
789 the REE tetrad effect in Evidence from the Qianlishan and Baerzhe granites: *Granites, China*.
790 *Geochemical Journal*, 36(6): 527-543.
- 791 Zimanowski, B., 2001. Phreatomagmatic explosions. In: Freundt, A., Rossi, M. (Eds.), *From magma to*
792 *tephra: modelling physical processes of explosive volcanic eruptions*. Elsevier Science,
793 Amsterdam, pp. 25-53.

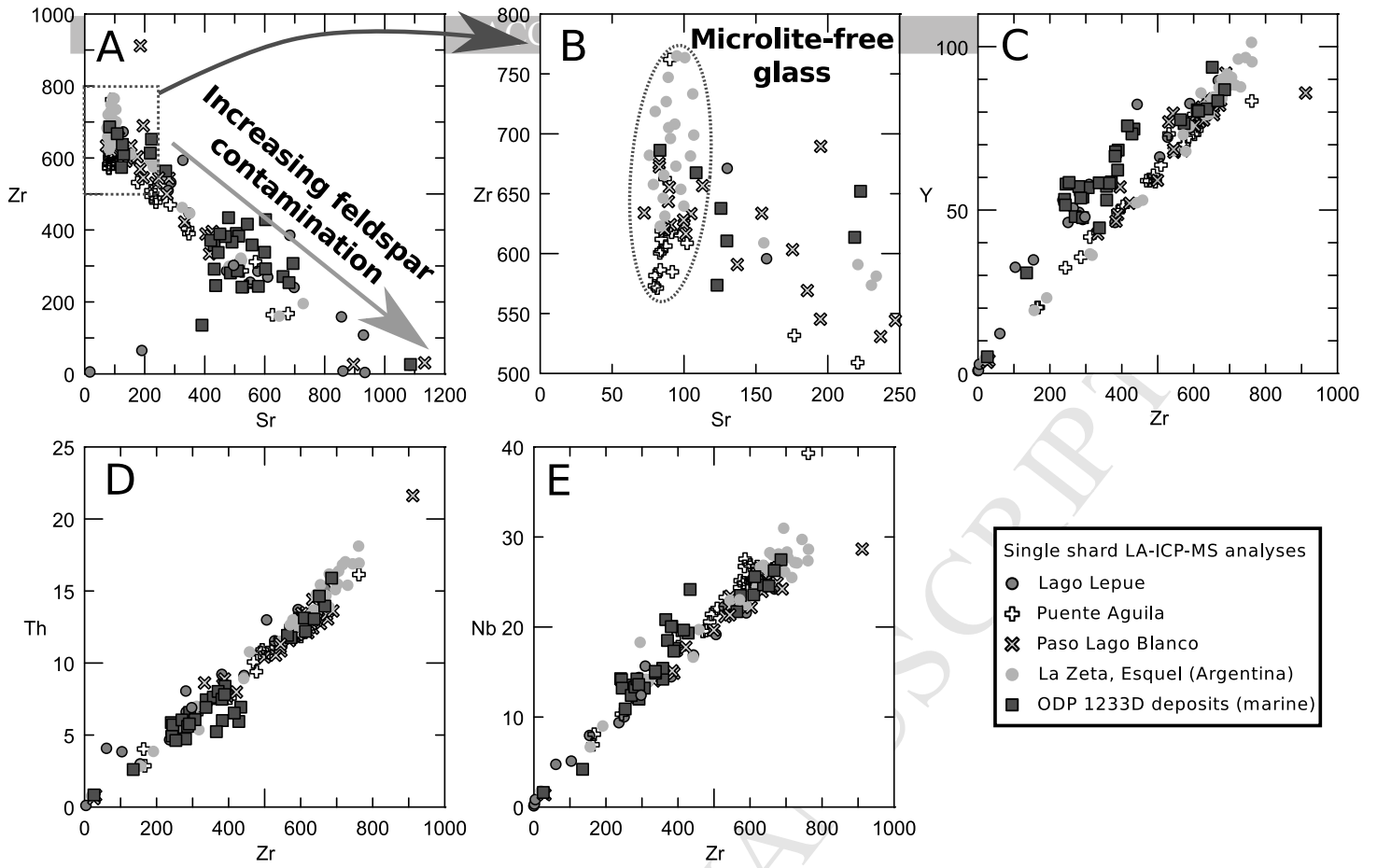
794







ACCEPTED



ACCEPTED MANUSCRIPT

